Journal of the European Ceramic Society 17 (1997) 1715–1723

PII: S0955-2219(97)00043-5
0955-2219/97/$17.00

Sintering of Industrial Mullites

L. Montanaro, J. M. Tulliani, C. Perrot & A. Negro

Department of Materials Science and Chemical Engineering - FERMAP, Politecnico of Torino, Corso Duca degli Abruzzi, 24, 10129 Torino, Italy

(Received 14 March 1996; revised version received 11 February 1997; accepted 17 February 1997)

Abstract

Two mullite powders, different in chemical and morphological characteristics, were compared with respect to their sinterability. For the development of a low-cost sintering step, MgO was added as sintering aid and its content was optimized for both mullites: the enhancement in sintering was imputed to a liquid phase formation. The two mullites presented a strongly different sinterability; the one gave rise to high density sintered bodies while the other, even after a grinding step which made its particle size distribution similar to that of the first, did not reach high final density. In both mullites, there was a pre-existing glassy phase: the strong influence of its content, composition and spatial distribution on the sintering behaviour was demonstrated. For better clarifying the action of the sintering aid, the glassy phase was eliminated by HF washing and the sintering behaviour of washed and unwashed samples with added MgO was compared. The contribution of MgO during sintering as well as the new phase formation in the sintered bodies seem to be linked to the alumina and impurity content of the mullites. © *1997 Elsevier Science Limited.*

1 Introduction

Mullite is the only intermediate stable compound in the SiO_2–Al_2O_3 system. Its properties such as high melting point (> 1800°C), low thermal expansion ($4{\cdot}5 \div 5{\cdot}6 \times 10^{-6}\,°C^{-1}$), good thermal shock fracture resistance, low true density ($3{\cdot}16 \div 3{\cdot}22\,g\,cm^{-3}$), high creep resistence and good chemical stability can be compared with the properties of Si_3N_4 and SiC in terms of being a candidate for high temperature structural materials applications.[1]

Thus mullite, like cordierite, silicon carbide and aluminium titanate, has been proposed for filters for diesel exhaust emissions.[2] These filters can have a honeycomb structure, produced by extrusion,[3] or a foam structure, developed from a polymeric sponge.[4]

Since the final aim of this research is the preparation of filters based on a mullite foam obtained by impregnation of a polymeric sponge and subsequent sintering, commercial powders able to cover the polymeric walls homogeneously and to sinter to high density at a relatively low temperature and in a short time are required. In a previous work,[5] some explorative tests have been performed to verify the ability of ceramic powders to give an appropriate coating on the walls of a poly(urethane) sponge. On the basis of these tests, two mullites were chosen for further investigations.

This paper deals with the comparison between these mullites which have different impurity levels and different chemico-physical and morphological characteristics; it concerns their sintering behaviour with and without a sintering aid. The need for this study comes from the fact that, even if many studies[6–13] have been recently carried out on mullite in order to enhance its mechanical behaviour and toughness, most refer to reaction sintering between zircon and alumina for producing zirconia-toughened mullite and only a few researches have been devoted[1,12,13] to the sintering behaviour of mullite itself: the latter researches principally concern the effect of sintering temperature on the microstructure and strength of dense mullite obtained from sol-gel powders, i.e. from very pure powders, far from the composition of common commercial products.

2 Materials and methods

The mullite powders, labelled from now on A (supplier VAW, Germany; type M72) and B (supplier Baikowski, France; type SA 193 CR) were characterized by chemical analysis (induction coupled plasma–atomic emission spectroscopy, ICP-AES) to complete the data given by the suppliers,

X-ray diffraction (XRD) (Philips PW 1710, Cu Kα radiation), laser granulometry (Malvern Instruments 3600D) and scanning electron microscopy (SEM) (Hitachi 2300).

It is well known that the sintering of mullite requires high temperatures and long treatments or the addition of a sintering aid, owing to the high activation energy for ion diffusion through the mullite lattice (702 kJ mol^{-1}).[14] Since the mass production of diesel particulate filters requires the development of a low-cost sintering step, i.e. a pressureless, low temperature and short-time sintering, it was necessary to use an appropriate sintering aid and optimize its content. On the ground of literature suggestions,[1,8,13,15] MgO was chosen.

Mullite–MgO mixtures in the compositional range between 0 and 3 wt% MgO[1,13] were prepared by ultrasonic homogeneization of alcoholic suspensions.

In order to study the sintering behaviour as a function of composition, bars of mullite powders with and without MgO were obtained by uniaxial pressing at 70 MPa and investigated by dilatometric analysis (Netzsch dilatometer 402 ED; heating and cooling rate of 10°C min^{-1} up to 1550°C).

The microstructures of all the sintered bodies were investigated by SEM observations after polishing and thermal etching. In addition, after sintering, XRD was performed to identify new phase formation.

3 Results

3.1 Powder characterization

In Table 1, the data of the chemical analysis of the mullite powders are presented. The two powders strongly differ in chemical purity; alumina and silica content, glassy phase percentage (about 11·1 and 5·3 wt% of glassy phase, respectively, in mullites A and B) were determined following the procedure described in the literature.[16,17]

The compositions of the glassy phases present in mullites A and B are given in Table 2. From the above results, it clearly appears that not only the percent amount of glassy phase, but also their mean compositions are quite different. The silica/alumina ratio is different in the two glassy phases (1·23 and 1·69 for mullites A and B, respectively) and it is very far from the mullite composition. The amounts of Fe_2O_3, Na_2O and K_2O are strongly higher in the glassy phase present in mullite A.

From the data given in Tables 1 and 2, it was possible to obtain the silica/alumina ratio in the crystalline portion of the mullites, which is presented in Table 3, together with the relative Al_2O_3 and SiO_2 weight percentages (without considering the impurity content).

From the literature data,[18] mullite A may be classified in the mullite–alumina phase region of the silica–alumina phase diagram, while mullite B is closer to the mullite solid solution range.

Other significant differences were shown. The two powders also differ in particle size distribution, as shown in Fig. 1: the mean particle size of mullites A and B were, respectively, about 10 and

Table 1. Composition of the mullite powders (values are given as wt%)

	A	*B*
Al_2O_3 *	70·66	72·17
SiO_2 *	23·96	26·10
Fe_2O_3	0·4	0·014
TiO_2	0·2	n.e.
Na_2O	n.e.	0·07
$Na_2O + K_2O$	0·5	n.e.
$CaO + MgO$	0·3	0·09

n.e. = not evaluated
*Analysis performed by Dept. Analytical Chemistry, University, Torino, Italy.

Table 2. Composition of the glassy phase present in the mullite powders (values are given as wt%)

	A	*B*
Al_2O_3	39·8	35·7
SiO_2	48·9	60·5
MgO	0·39	0·1
ZrO_2	2·3	1·87
TiO_2	0·58	—
Fe_2O_3	1·45	0·11
Na_2O	1·24	0·8
K_2O	4·74	—

Analysis performed by the Dept. Analytical Chemistry, University, Torino, Italy.

Table 3. Composition of the crystalline portion of mullites (values are given as wt%)

	A	*B*
SiO_2/Al_2O_3	0·28	0·33
Al_2O_3	78·1	75·4
SiO_2	21·9	24·6

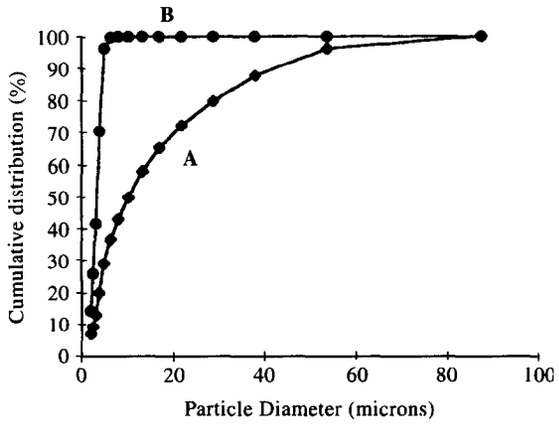

Fig. 1. Particle size distribution of the two powders.

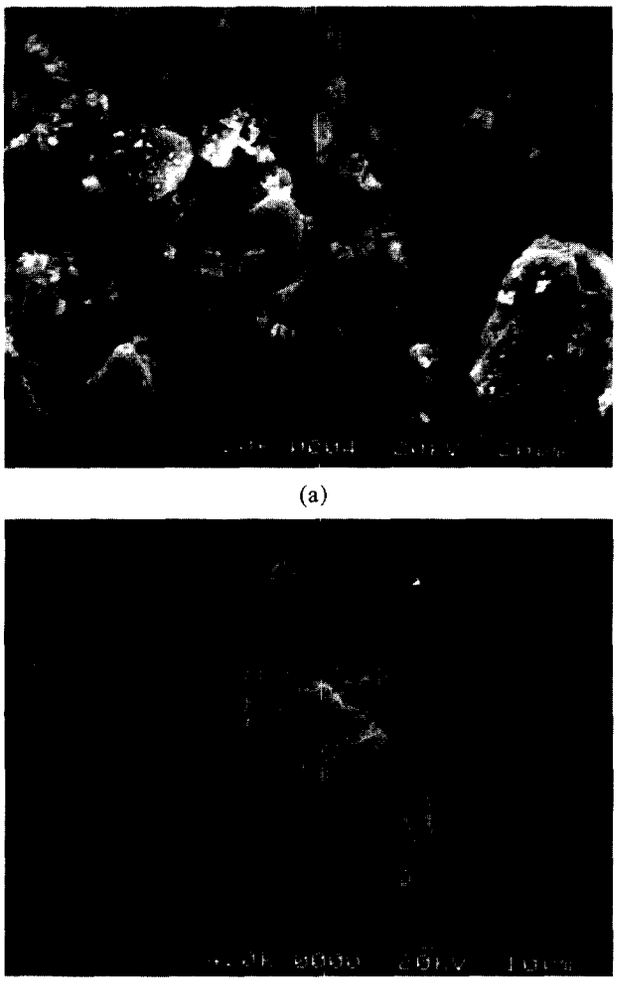

(a) (b)

Fig. 2. SEM morphology of the two powders: (a) A; (b) B.

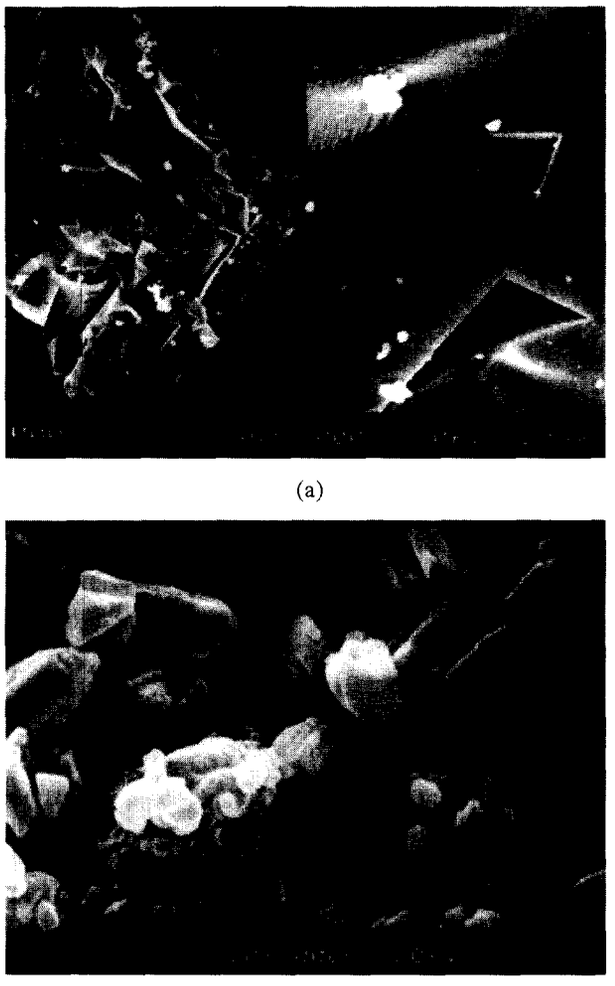

(a) (b)

Fig. 3. SEM micrographs of HF-etched mullite powders: (a) A; (b) B.

4 μm. In powder A, irregularly shaped hard agglomerates are mainly present [Fig. 2(a)]. In contrast, mullite B presents a narrower particle size distribution with an upper limit of 8 μm; it is formed by only few agglomerates and needle-like grains [Fig. 2(b)]. MgO presents a mean particle size of about 7 μm.

SEM images of the powders A and B after chemical etching, performed for 6 h in 2 vol% HF,[16,17] are presented in Fig. 3. It clearly appears that the chemical etching slightly modifies the microstructure of B grains [Fig. 3(b)]; in contrast, the morphology of powder A is strongly affected: large polyhedric cavities appear on the surface of the particles [Fig. 3(a)]. It can be supposed that a thin film of glassy phase covers the grains of mullite B, whereas the glassy phase is preferentially located in distinct regions of the agglomerates of powder A.

3.2 Sintering behaviour

3.2.1. The effect of MgO additive

The green density after uniaxial pressing was 60 and 44% of the theoretical value for mullites A and B, respectively. The higher green density of compact A can be imputed to its particle size distribution and, particularly, to the presence of a large amount of fine particles able to fill the intergranular voids between the larger particles.

The dilatometric behaviour of mullites with and without MgO is shown in Fig. 4. As clearly appears in this figure, initial-stage sintering without the sintering aid was very poor and similar for the two mullites, even if the particle size distributions of the powders are quite different. Conversely, the MgO additions induced a shift of the sintering onset temperature to lower temperature, at least 100°C less, for both mullites and, in addition, they enhanced the sintering rate and shrinkage, expecially for mullite B.

From the results of dilatometric measurements, from preliminary tests[5] and in the perspective of industrial production of mullite foams, a temperature of 1550°C was chosen as the sintering condition.

The curves of theoretical density percentage versus time are presented in Fig. 5. For pure mullites, sintering at 1550°C achieves relative densities of 63

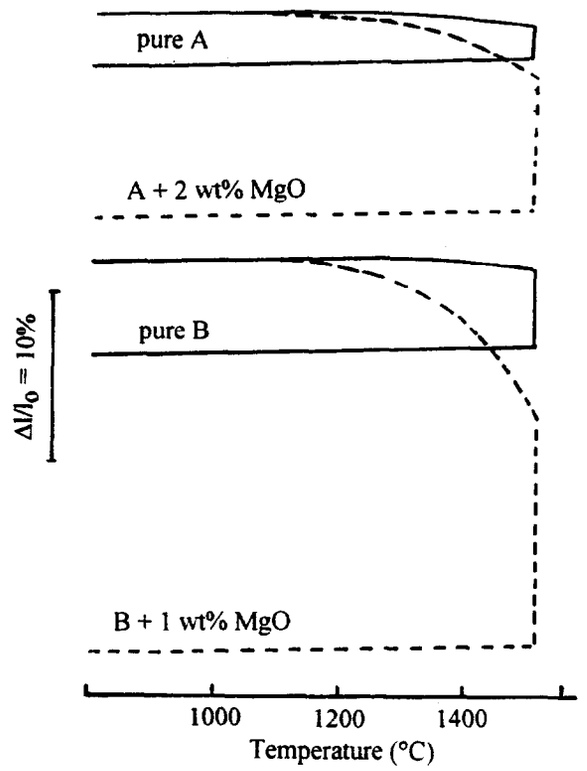

Fig. 4. Dilatometric behaviour of mullites with and without MgO: (a) A; (b) B.

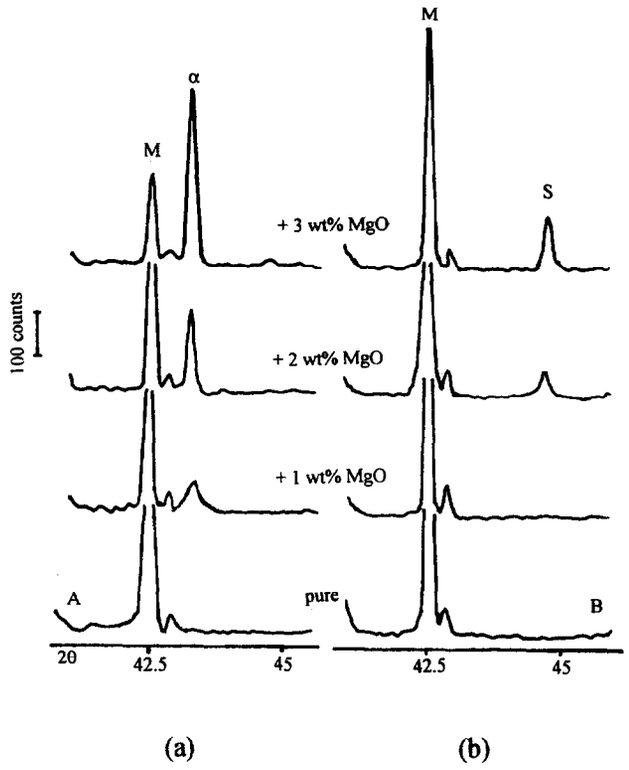

Fig. 6. XRD patterns of sintered mullites with and without MgO: (a) A; (b) B ($\alpha = \alpha$ alumina; S = Mg–Al spinel).

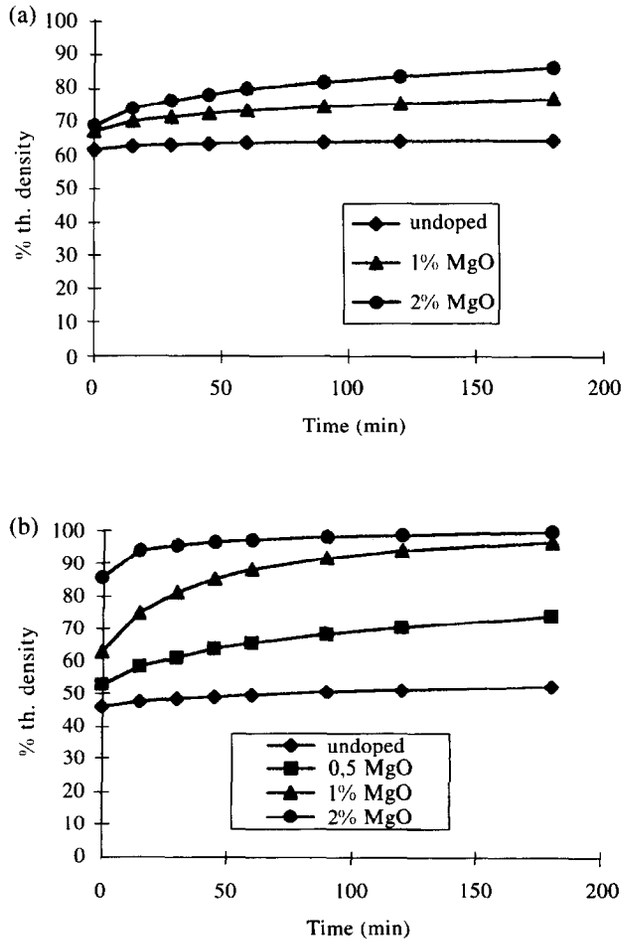

Fig. 5. Evolution of theoretical density percentage versus time at 1550°C for mullites with and without MgO: (a) A; (b) B.

and 50%, respectively, for powders A and B. Addition of 1 wt% MgO achieves a final density higher than 98% of the theoretical value in sample B, while powder A added with 2 wt% MgO reaches 86% of the theoretical density.

The XRD analyses, performed on the pellets sintered at 1550°C for 3 h, showed the appearance of secondary phases due to the presence of the sintering aid (Fig. 6). In the case of mullite A, the pattern of doped samples presents the peaks of α alumina. The higher is the content of MgO, the higher the intensity of α alumina peaks. From addition of 3 wt% MgO, Mg–Al spinel traces were also observed. A different behaviour is presented by mullite B. Starting from the addition of 2 wt% MgO, peaks imputed to spinel are present on XRD patterns, but there is no evidence of α alumina formation.

Microstructural observations showed that 1 wt% MgO-doped mullite A [Fig. 7(a)] was badly sintered: dense regions are separated by large pores. With increasing MgO content, mullite A sintered better but its microstructure was inhomogeneous: small grains are present near to larger grains, having up to 20 microns in length [Fig. 7(b)]. In addition, when 3 wt% MgO was added, glassy regions appeared in the multiple-grain junctions.

The microstructure of mullite B, with 1 wt% MgO, has less porosity and grains whose size is uniform and less than 4 microns [Fig. 7(c)]. The

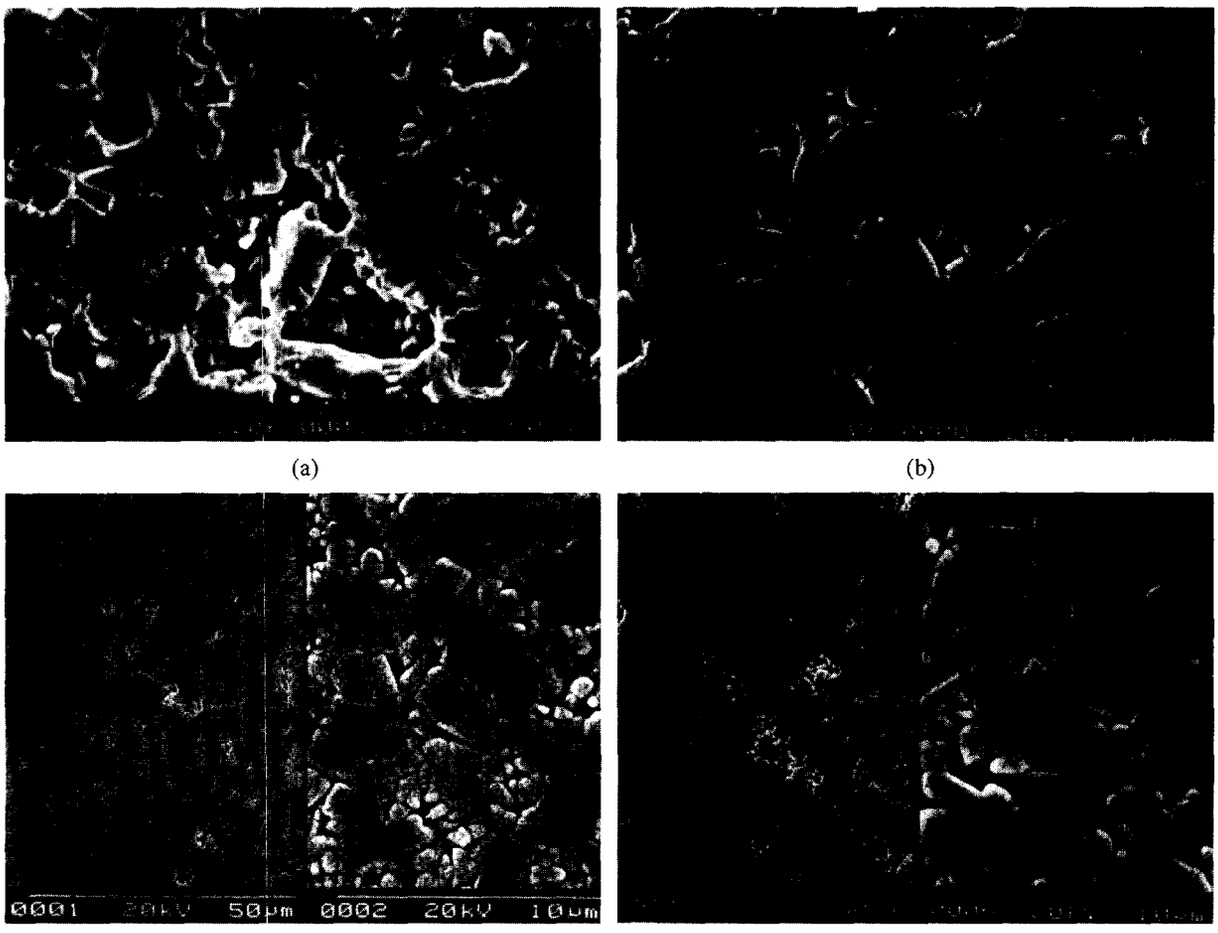

Fig. 7. SEM micrographs of sintered mullites: (a) 1 wt% MgO-doped mullite A; (b) 2 wt% MgO-doped mullite A; (c) 1 wt% MgO-doped mullite B; (d) 2 wt% MgO-doped mullite B.

addition of 2 or 3 wt% MgO did not significantly change the microstructure [Fig. 7(d)]. There is evidence of grain growth and appearance of more elongated grains (up to 10 microns in length).

The above results indicate the strong influence of MgO during sintering of both mullites, but the understanding of this influence is made hard by the complexity of the systems. During sintering of these commercial powders, many parameters, e.g. their particle size distribution, their impurity level and content, composition and spatial distribution of their glassy phase, can play a role. In order to clarify the influence of these parameters and to draw out the effect of the sintering aid, the two mullites were compared when having a similar particle size distribution and, above all, when the pre-existing glassy phase was eliminated.

3.2.2. The effect of the particle size distribution

Powder A was ground in alcoholic suspension by a planetary mill to lower its particle size distribution and to make it comparable with that of powder B: after grinding, the mean diameter was 5 μm, and the size at 10 and 90% of the distribution was, respectively, 1·5 and 10 μm.

The dilatometric curve of ground A with 2 wt% MgO is presented in Fig. 8 and compared to an unground sample. The shrinkage starts at a lower temperature and the densification behavior of ground A is similar to that of sample B added with 1 wt% MgO (of Fig. 4), even if the linear shrinkage in the isothermal step is less significant (about 11·5%).

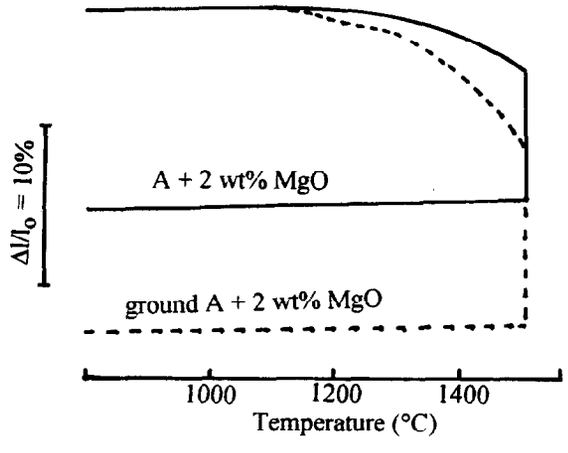

Fig. 8. Dilatometric behaviour of ground mullite A added with 2 wt% MgO.

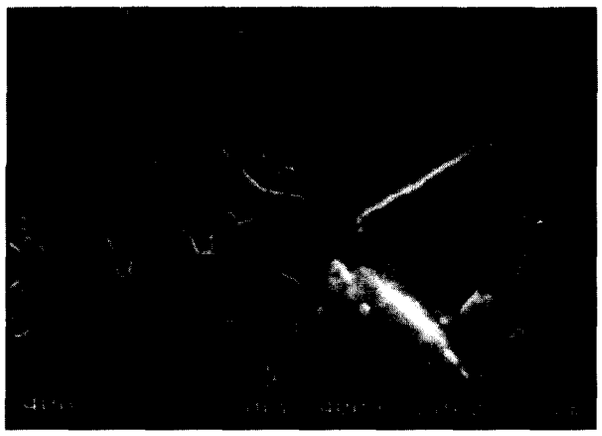

Fig. 9. SEM micrograph of sintered 2 wt% MgO-doped ground mullite A: general view and detail of a glassy phase at a multiple-grain junction.

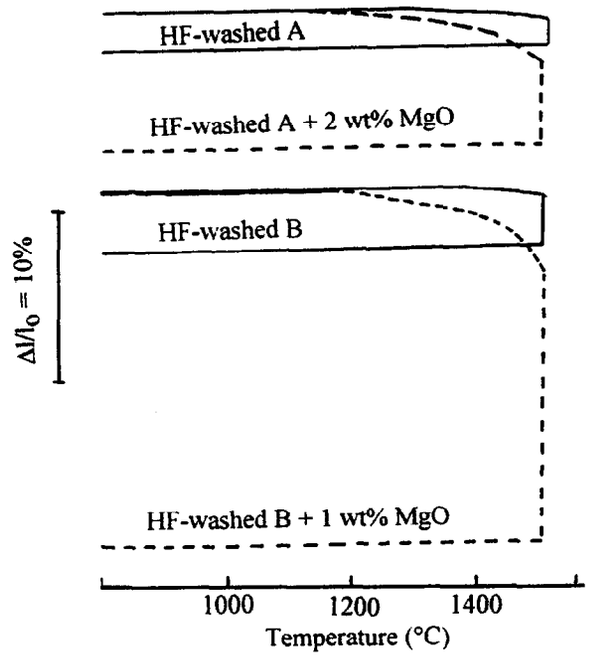

Fig. 10. Dilatometric behaviour of HF-etched mullite powders with and without MgO.

The green and final density were, respectively, 48 and 91% of the theoretical value, this latter definitely higher than that of the unground sample (about 86%). Despite the beneficial effect induced by grinding, the sinterability of powder A remains lower than powder B and for enhancing sinterability the need for a double amount of MgO (2 wt%) still remains.

The microstructure of the sintered body, shown in Fig. 9, confirmed the better sinterability of ground powder A, even if its microstructure remained inhomogeneous: the grain size is strongly variable, from 2 to about 25 μm; pores of about 10 μm in length and a glassy phase at multiple-grain junctions are evident.

The glassy phase appeared more homogeneously distributed due to the presence of glassy pockets present inside the agglomerates: this glass is able to fill up the residual porosity more efficiently than in the unground sintered sample.

In conclusion, the role of the particle size distribution is clear but not sufficient in itself to justify the difference in densification behaviour between A and B.

3.2.3. The sintering behaviour of the HF-washed powders

The dilatometric behaviour of mullites A and B, without the glassy phase, has been investigated using the same heat treatment already described. Bars of mullites with and without MgO were also prepared in this case.

The results presented in Fig. 10 show that the mullites A and B, after HF washing, present a sintering behaviour similar to that of the unwashed powders (Fig. 4). The starting shrinkage temperature is not strongly affected by chemical etching of the powders. During the isotherm step there is a shrinkage reduction, more evident for mullite B: in this case, the mullite B presents a shrinkage of 5% before washing and 3% after washing.

The better sinterability of undoped washed B can be imputed to the more favourable particle size distribution and silica/alumina ratio: in fact, as demonstrated by Sacks and Pasks[19] for solid-state sintering of mullite, a sharp decrease in densification rate is observed on transition from mullite solid solution range to mullite–alumina phase region, i.e. in our case in the transition from powder B to A.

The different behaviour of the two powders is more evident when they are sintered, after HF washing, in the presence of the sintering aid. The starting shrinkage temperature increases for both mullites after HF treatment: this phenomenon is more evident for mullite B; there is also a difference in shrinkage during the isotherm step. The percent linear shrinkage in HF-washed mullites is lower than in the unwashed samples. The values are, respectively: for mullite A, 8·5 and 12%; for mullite B, 21 and 23%.

The worse sinterability of mullite A without the glassy phase is also underlined by the microstructural observations of the sintered bodies. The presence of interconnecting pores having dimension sometimes higher than 20 μm and the appearance of partially sintered grains were clearly observed. On the contrary, the good sintering behaviour of the washed mullite B was confirmed by the observation of a reduced amount of pores, whose dimension does not exceed 2 μm.

The comparison between the washed and unwashed sample sintering behaviour provides an

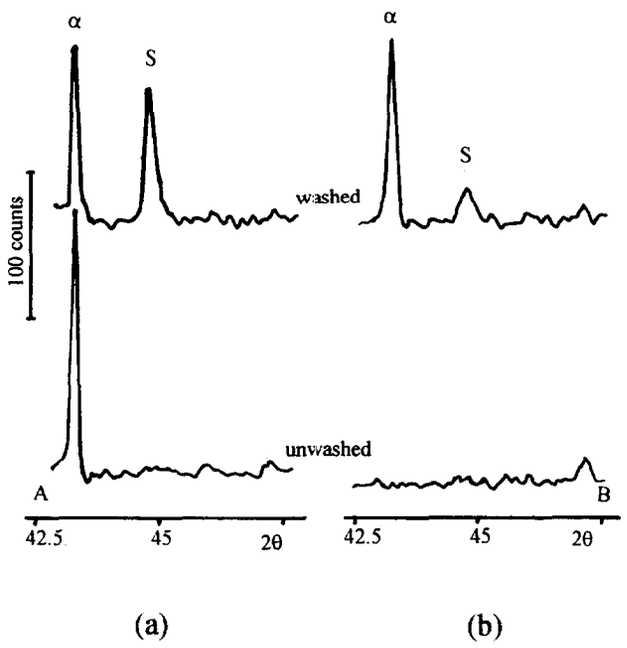

Fig. 11. XRD patterns of HF-washed mullites, compared with the unwashed samples similarly added: (a) A + 2 wt% MgO; (b) B + 1 wt% MgO ($\alpha = \alpha$ alumina; S = Mg–Al spinel).

interpretative tool for clarifying the effect of the pre-existing glassy phase. In its presence, the sinterability of both mullite powders is enhanced: this favourable effect would be expected because a glassy phase is able to lower the interfacial energies[19] and to lead to a sintering in the presence of a viscous or liquid phase. In this case, however, the two glassy phases are characterized by a different amount, composition and local distribution in the two mullites: therefore, they do not act similarly during sintering. In B, the glassy phase is more homogeneously distributed all around the mullite grains, as confirmed by SEM observations (Fig. 3) and thus can take a more effective and active part in sintering. In addition, its alumina content (Table 2) is lower than that of the glassy phase present in A. That assures the formation of a lower viscosity and higher wettability liquid during sintering.

4 Discussion

When the pre-existing glassy phase is eliminated by HF washing, the role of the sintering aid can be better understood. In this case, we can consider the $MgO–Al_2O_3–SiO_2$ phase diagram:[20] due to the presence of MgO, the formation of a liquid phase is expected at 1482°C for a composition beginning in the mullite–spinel–sapphirine phase field and at 1578°C for one beginning in the corundum–mullite–spinel field. Although these correspond to mullites B and A, respectively, (with added MgO), the presence of residual impurities is expected to reduce these temperatures further. Nonetheless, the faster densification in mullite B at the firing temperature (1550°C) can be understood. The higher alumina content of A bestows a more refractory behaviour.

The phase diagram can explain the new phase formation, and also the liquid phase formed during sintering acts as a solvent of MgO, enhancing its diffusion and the homogeneization of its content inside the mullite compacts.

Both washed mullites with added MgO (mullite A + 2 wt% MgO; mullite B + 1 wt% MgO) show the presence of α alumina and Mg–Al spinel peaks (Fig. 11). Above the peritectic point, mullite, α alumina and liquid are expected. Below the peritectic, mullite, spinel and liquid should be present. It is therefore reasonable that, with conventional cooling, non-equilibrium presence of mullite, alumina and spinel should occur.

Comparing the new phases formed by the washed and unwashed samples (Figs 6 and 11), the following conclusions can be drawn.

For the washed B with added MgO, a liquid phase is formed during sintering having, on the ground of the phase diagram, a higher silica and lower alumina content than the starting mullite. Its formation leads to a local modification of the stoichiometry of mullite from alumina/mullite molar ratio close to 3:2 to higher values. A scheme of this phenomenon is proposed in Fig. 12. Powder B is relatively pure after washing and it can be supposed that, in the phase diagram, the peritectic point (1578°C) is not considerably lowered. Thus, on cooling, we should expect the formation of spinel near mullite, but the system probably has not time to reach an equilibrium condition, leading to residual alumina. In the case of doped washed A, due to the higher content of alumina of the crystalline mullite and to the higher content of MgO (2 wt% instead of 1 wt%), on cooling this mixture yields a higher content of α alumina. More complicated is the description of the behaviour in the case of the unwashed mullite because of the presence of the pre-existing glassy phase.

For unwashed A with added MgO, the high impurity content probably leads to a lowering of the peritectic point. This effect, together with the considerable amount of glassy phase and its higher alumina content leads, to the α alumina formation near mullite, on cooling.

For unwashed B with added MgO, the limited impurity content and lower amount of pre-existing glassy phase probably enables a more limited lowering of the peritectic point. This condition, together with a lower alumina concentration in the pre-existing glassy phase which can still act as alumina

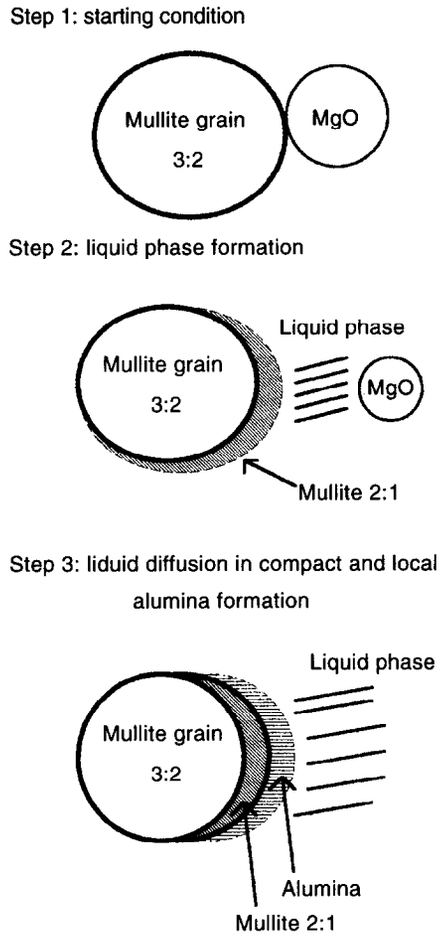

Fig. 12. Scheme of the interaction between MgO and mullite grains during sintering.

solvent, leads to the appearance of only spinel near mullite, starting from significant MgO addition (2 wt% or more).

5 Conclusions

The sintering behaviour of two commercial powders, A and B, to be used for ceramic foams production was investigated. These powders differ in particle size distribution; silica/alumina ratio and impurity level in the mullite phase; content, composition and spatial distribution of a glassy phase. All these parameters are able to influence their sinterability.

Starting from the experimental results the following conclusions can be drawn:

(a) A and B strongly differ in sinterability. Powder B reached about the theoretical density after sintering at 1550°C, by adding 1 wt% MgO as sintering aid. Even if a double quantity of MgO was added to powder A, only 86% of the theoretical density was obtained; higher MgO content caused distorsions in the sintered samples;

(b) the different particle size distribution was demonstrated to be not the only cause of the different sinterability. After a grinding step which made the particle size distribution of A similar to that of powder B, the difference in sintering behaviour still remained, even if an increase in final density of sintered A (from 86 to 91%) was obtained;

(c) in both mullites, a pre-existing glassy phase enhances their sinterability. Moreover, the glassy phase in B appears more efficient due to its highly homogeneous distribution all around the mullite grains and the lower alumina amount which can lead to a less viscous liquid having higher wettability;

(d) when the pre-existing glassy phase was eliminated by HF washing, the formation of a liquid phase during heat treatment able to enhance the powder sinterability was demonstrated. The mullite A, with higher alumina content in the crystalline portion, showed the lower sinterability;

(e) the new phase formation during cooling (the appearance of Mg–Al spinel and α alumina, differently as a function of washed or unwashed, doped or undoped samples) is understandable in terms of the $MgO–Al_2O_3–SiO_2$ phase diagram and its possible modifications, namely of the temperature of the peritectic point (1578°C), induced by the impurities and glassy phase present in the starting powders.

Acknowledgements

The authors are greatly indebted to CEE-HCM Program for the financial support and the grant given to Dr Perrot, to Conseil Régional de la Région Provence–Alpes–Côte d'Azur for the grant to Dr Tulliani, and to Professor Fantozzi, Professor Esnouf, and Dr Thollet of G.E.M.P.P.M. of the INSA, Lyon for helpful discussion.

References

1. Somiya, S. and Hirata, Y., Mullite powder technology and applications in Japan. *Am. Ceram. Soc. Bull.*, 1991, **70**, 1624–1632.
2. Tulliani, J. M., Montanaro, L., Borello, C. and Demaestri, P. P., Filtri ceramici per il controllo delle emissioni di motori Diesel: presente e futuro. *Ceramurgia*, 1995, **25**, 81–90.
3. Lachman, I. M., Bagley, R. D. and Lewis, R. M., Thermal expansion of extruded cordierite ceramics. *Am. Ceram. Soc. Bull.*, 1981, **60**, 202–205.
4. Saggio-Woyansky, J., Scott, C. E. and Minnear, W. P., Processing of porous ceramics. *Am. Ceram. Soc. Bull.*, 1992, **71**, 1674–1682.

5. Tulliani, J. M., Montanaro, L. and Borello, C., Open pore mullite foams for Diesel particulate filtration, In *Proc. IV Euro Ceramics, Basic Science, Trends in Emerging Materials and Applications*, vol.4, ed. A. Bellosi. Faenza Editrice, Faenza, Italy, 1995, pp. 493–500
6. Di Rupo, E., Gilbart, E., Carruthers, T. G. and Brook, R..J., Reaction hot-pressing of zircon-alumina mixtures. *Journal of Mater. Sci.*, 1979, **14**, 705–711.
7. Pena, P., Miranzo, P., Moya, J. S. and De Aza, S., Multicomponent toughened ceramic materials obtained by reaction sintering. Part 1: ZrO_2–Al_2O_3 –SiO_2–CaO system. *Journal of Mater. Sci.*, 1985, **20**, 2011–2022.
8. Miranzo, P., Pena, P., Moya, J. S. and De Aza, S., Multicomponent toughened ceramic materials obtained by reaction sintering. Part 2: ZrO_2–Al_2O_3–SiO_2–MgO system. *Journal of Mater. Sci.*, 1985, **20**, 2702–2710.
9. Melo, M. F., Moya, J. S., Pena, P. and De Aza, S., Multicomponent toughened ceramic materials obtained by reaction sintering. Part 3: ZrO_2–Al_2O_3–SiO_2–TiO_2 system. *Journal of Mater. Sci.*, 1985, **20**, 2711–2718.
10. Leriche, A., Cambier, F. and Brook, R. J., Study of some factors influencing the microstructural developement of mullite-zirconia composites obtained by reaction sintering. *Special Ceramics 8, Br. Ceram. Proc.*, 1986, **37**, 167–177.
11. Torrecillas, R., Elaboration, caractérisation microstructurale et mécanique des composites céramiques à base mullite et zircone. Ph.D.Thesis, INSA, Lyon, 1994.
12. Ishibashi, N., Takara, K., Kobayashi, H., Mitamura, T. and Akiba, T., Effect of metallic salt additives on the properties of mullite sintered bodies. In *Extended Abstracts of Annual Meeting*. The Ceramic Society of Japan, 1989, 2C48.
13. Ismail, M. G. M. U., Tsunatori, H. and Nakai, Z., Preparation of MgO-doped mullite by sol-gel method, Powder characteristics and sintering. *Journal of Mater. Sci.*, 1990, **25**, 2619–2625.
14. Skoog, A. and Moore, R., Refractory of the past for the future: Mullite and its use as bonding phase. *Am. Ceram. Soc. Bull.*, 1988, **67**, 1180–1185.
15. Srikrishna, K., Thomas, G. and Moya, J. S., Sintering additives for mullite/zirconia composites. *Adv. Ceram., Science and Technology of Zirconia III*, 1988, **24**, 277–286.
16. Murat, M., Arnaud, Y., El Moussaouiti, M. and Comel, C., Détermination des teneurs en alumino-silicates cristallisées et amorphes dans les cendres volantes et les mullites synthétiques. *Silicates Ind.*, 1984, **6**, 127–135.
17. Murat, M. and Driouche, M., Characterisation of the crystallinity of silicates by dissolution conductimetry. *Journal of Europ. Ceram. Soc.*, 1990, **6**, 73–83.
18. Klug, F. J., Prochazka, S. and Doremus, R. H., Alumina-Silica phase diagram in the mullite region. *Journal of Am. Ceram. Soc.*, 1987, **70**, 750–759.
19. Sacks, M. D. and Pask, J. A., Sintering of mullite-containing materials: I, Effect of composition. *Journal of Am. Ceram. Soc.*, 1982, **65**, 65–70.
20. *Phase Equilibrium Diagrams of Oxide Systems*, Plate 3, Fig. 712, American Ceramic Society and the Edward Orton Jr, Ceramic Foundation, 1960.